AGU100 ADVANCING EARTH AND SPACE SCIENCE

Geophysical Research Letters

RESEARCH LETTER

10.1029/2018GL077526

Intense Granular Sheetflow in Steep Streams

Marisa C. Palucis[1,2], Tom Ulizio[1], Brian Fuller[1], and Michael P. Lamb[1]

[1]Division of Geological and Planetary Sciences, California Institute of Technology, Pasadena, CA, USA, [2]Department of Earth Sciences, Dartmouth College, Hanover, NH, USA

Key Points:
- We conducted flume experiments with bed gradients of 10–30% under high Shields stresses where models predict riverbeds should fail
- Instead of bed failure, we observed development of a highly concentrated sheetflow layer beneath a dilute bedload layer
- Sheetflows were thicker on steeper slopes and had nonlinear velocity profiles that scale with bed shear velocity

Supporting Information:
- Supporting Information S1
- Table S1
- Movie S1

Correspondence to:
M. C. Palucis,
marisa.c.palucis@dartmouth.edu

Citation:
Palucis, M. C., Ulizio, T., Fuller, B., & Lamb, M. P. (2018). Intense granular sheetflow in steep streams. *Geophysical Research Letters*, *45*, 5509–5517. https://doi.org/10.1029/2018GL077526

Received 8 FEB 2018
Accepted 22 MAY 2018
Accepted article online 29 MAY 2018
Published online 9 JUN 2018

Abstract Quantifying sediment transport rates in mountainous streams is important for hazard prediction, stream restoration, and landscape evolution. While much of the channel network has steep bed slopes, little is known about the mechanisms of sediment transport for bed slopes between $10\% < S < 30\%$, where both fluvial transport and debris flows occur. To explore these slopes, we performed experiments in a 12-m-long sediment recirculating flume with a nearly uniform gravel bed. At 20% and 30% bed gradients, we observed a 4-to-10 particle-diameter thick, highly concentrated sheetflow layer between the static bed below and the more dilute bedload layer above. Sheetflow thickness increased with steeper bed slopes, and particle velocities increased with bed shear velocity. Sheetflows occurred at Shields stresses close to the predicted bedload-to-debris flow transition, suggesting a change of behavior from bedload to sheetflow to debris flow as the bed steepens.

Plain Language Summary Sediment transport within mountain rivers controls their shape, supplies sediment downstream for aquatic habitat, and can be a major hazard to life and infrastructure. Sediment tends to move by river processes where channel slopes are relatively gentle and by debris flows at very steep gradients; however, the mode of transport is not understood for the range of bed slopes in between. To address this knowledge gap, we performed laboratory experiments in a steep, 12-m-long flume to determine when and where river processes transition to debris flows. Surprisingly, we found a distinct third mode of transport developed called sheetflow. Sheetflows are dense granular slurries that are a hybrid between traditional river transport and debris flows. They occur on lower gradient sandy beds under high shear stresses but have not been previously documented in steep mountain streams. We map the parameter space where sheetflows occur, and quantify controls on their thickness and particle velocities. Our results indicate that there is a continuum of behavior as a channel bed steepens, from river to sheetflow to debris flow processes, which has significant implications for predicting sediment fluxes and channel bed morphology in mountain streams.

1. Introduction

Sediment transport in steep mountain channels controls channel morphology (Montgomery & Buffington, 1997; Palucis & Lamb, 2017) and landscape evolution under changing climatic and tectonic regimes (Montgomery & Brandon, 2002; Stock & Dietrich, 2003), and can pose major hazards to life and infrastructure (Jakob et al., 2005; Lamb & Fonstad, 2010). However, little is known regarding the mechanisms by which sediment is entrained and transported in steep mountain channels. Recent field and experimental work suggests that fluvial transport is less effective with increasing bed slope due to the presence of immobile (or rarely mobile) boulders and channel forms, shallow and rough flows, grain hiding, partial transport, and grains that protrude through the flow (Church & Hassan, 2002; Lamb et al., 2008, 2017a, 2017ab; Mao et al., 2008; Schneider et al., 2015; Yager et al., 2012). Even more uncertain is our understanding of the transition from fluvial processes to debris flows. Debris flows have significantly higher sediment concentrations, and both solid and fluid forces influence their downslope motion, making them destructive to both humans and infrastructure (Iverson, 1997; McArdell et al., 2007; Pierson, 1981; Takahashi, 1978). For channel bed slopes (S) less than ~3%, sediment is typically transported fluvially (e.g., Stock & Dietrich, 2003), and Prancevic et al. (2014) have shown through flume experiments that there exists a threshold slope, S_c, above which mass failure of the channel bed initiates a debris flow prior to any fluvial grain entrainment ($S_c \sim 40\%$). Due to limited field and flume observations, it is not clear what transport processes dominate at bed gradients from 3% to 40% (Cannon et al., 2001; Imaizumi et al., 2016; Montgomery & Buffington, 1997).

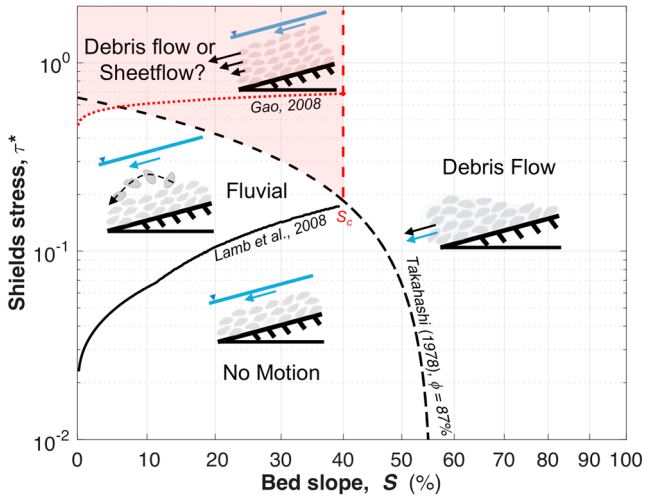

Figure 1. Hypothesized zones of sediment transport mode following Prancevic et al., 2014. The black arrows designate sediment motion, and the blue arrows designate fluid motion. Phase space boundaries are based on the initial motion criterion for bedload of Lamb et al. (2008) (solid black line), fluvial-to-debris flow transition from Takahashi (1978) (black dashed line), and the onset of sheetflow from Gao (2008), extrapolated to steep bed slopes using a slope-dependent critical Shields stress (Lamb et al., 2008). We tested the mode of transport at slopes less than S_c and large τ^* (shaded in red).

Prancevic et al. (2014) mapped out a theoretical phase space with zones of no motion, fluvial bedload transport, and bed failure resulting in debris flow using the models of Lamb et al. (2008) for fluvial transport and Takahashi (1978) for bed failure (Figure 1). Their transport phase space suggests that for a given bed slope less than S_c, increasing nondimensional bed stress, or Shields stress (τ^*), will result in a transition from bedload transport to bed failure; this hypothesis has yet to be tested. Another possibility is that an intense sheetflow layer will develop, similar to what has been observed in low gradient channels at high Shields stresses (Asano, 1993; Hanes & Bowen, 1985; Recking, 2009). Sheetflows on low bed slopes differ from debris flows on steep slopes in several ways. Under sheetflow conditions, a relatively thin layer of colliding grains, with a solids concentration (C_b) approaching that of the stationary bed, is transported below a dilute shear flow. While grain-grain interactions are thought to be important in transferring momentum within the sheetflow layer (Gotoh & Sakai, 1997), sediment transport is mainly driven by shear from the overlying water flow (e.g., Asano, 1993; Sumer et al., 1996; Wilson, 1989). In contrast, in debris flows, water and sediment are relatively well mixed throughout the flow depth; momentum is transferred simultaneously by grain friction, grain collisions, and viscous fluid flow; and the water-and-sediment slurry typically moves in surges, often leading with a granular snout (Iverson, 1997; Johnson et al., 2012; Kaitna et al., 2016). Flume and duct experiments conducted at lower bed slopes ($S < 3\%$) with sand-sized material and unidirectional flow suggest that the onset of sheetflow can occur for Shields stresses between 0.4 and 1 (Gao, 2008; Nnadi & Wilson, 1992; Pugh & Wilson, 1999), similar to the Shields stress criteria for bed failure at $S_c > 40\%$ (Prancevic et al., 2014). Currently, we lack observations of when and where bedload, sheetflow, and debris flows occur, and especially the transitions between these transport modes at bed slopes in between 3% and 40%.

We performed a series of flume experiments in the Earth Surface Dynamics laboratory at the California Institute of Technology to identify the transitions between bedload transport, sheetflow, and debris flows in a steep alluvial channel (i.e., S = 10%, 20%, and 30%) subject to steady, uniform water flow. In section 2 we discuss our methods and experimental setup, and in section 3 we present data suggesting that debris flows are not initiated below a critical slope under uniform water flow conditions, but rather sheetflow occurs. In section 4 we discuss how the sheetflow regime differs from bedload and debris flow regimes and explore what sets the sheetflow thickness and velocity distribution with depth.

2. Experimental Setup and Methodology

Seventy experimental runs were conducted in a 12-m-long, 0.18-m-wide tilting flume (Figure S1) with different combinations of bed slope and water discharge. The flume is equipped with a conveyor system capable of recirculating up to ~4 kg/s of gravel. All experiments used the same natural river gravels that were well-sorted, semiangular, and had a median grain diameter (D_{50}) of 5.4 mm and D_{84} (the grain size for which 84% of the grains are smaller) of 6.1 mm (Figure S2). This grain size was chosen to achieve high particle Reynolds numbers ($>10^3$),

$$Re_p = \sqrt{\frac{\tau}{\rho}}\frac{D_{50}}{\nu}, \tag{1}$$

where τ is the basal shear stress on the bed, ρ is the density of water, and ν is the kinematic viscosity of water, which also would be the case for gravel and coarser sediment in mountain streams (e.g., Trampush et al., 2014).

Prior to the start of each experiment, the alluvial bed was hand screeded to be planar. The bed was scanned at submillimeter vertical accuracy every 1 mm along the channel width and every 5 mm down-channel using

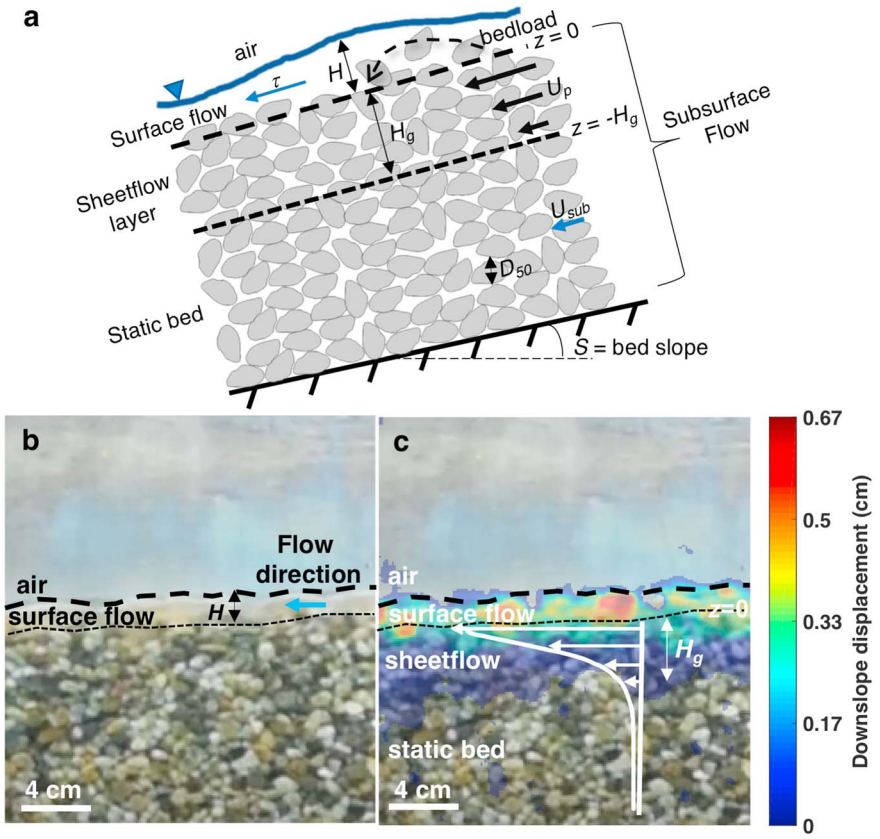

Figure 2. (a) Schematic showing zones of flow and sediment transport for the surface ($z > 0$) and the subsurface ($z < 0$) in which the blue arrows indicate water flow and the black arrows indicate particle velocities. The surface flow water depth is H, which exerts a bed shear stress τ. Particles transported in the surface flow are transported as bedload. A sheetflow layer may develop below the surface flow with thickness H_g and a particle velocity, U_p. U_{sub} is the mean fluid subsurface flow velocity. (b) Side-view image from experiment 67 (S = 30% and H = 1.3 cm) showing the top and bottom of the dilute surface flow layer, and the surface flow depth (H; Figure S3). (c) Same image as in panel b but overlain by a downslope particle displacement map and resulting measured particle velocity profile, U_p (z), generated from two successive images (taken 1/60 s apart).

a Keyence laser attached to a motorized cart. These scans were repeated during and after each experiment. Average bed thicknesses ranged from 20.6 to 21.4 cm in different experiments (Figure 2a). A single layer of grains was permanently fixed to the flume floor to prevent sliding along this boundary. During an experiment, the total inlet discharge (Q_t) and sediment supply (Q_s) were increased incrementally (by 5 to 10%) and held steady for ~10 min after each change until equilibrium conditions were reached, defined as the lack of aggradation or degradation of the bed, a steady alluvial bed slope, and input sediment fluxes approximately equaling output sediment fluxes. To prevent initial scour of the bed when increasing the total inlet discharge, sediment was fed from the hoppers for several minutes until sediment exiting the flume was able to recirculate back to the flume inlet; at this point, the hoppers were turned off and sediment was recirculated. Water discharge was measured using two in-line Rosemount magnetic flowmeters, and sediment flux was calculated based on sediment hopper and conveyor speeds, and from sediment trap measurements at the flume exit (Table S1).

Surface water discharge (Q_{sur}) was calculated at each equilibrium condition by taking the total inlet discharge measured from the flowmeters and subtracting the subsurface discharge through the permeable gravel bed (Q_{sub}). The subsurface discharge was determined by slowly increasing the discharge until surface flow was observed (Figure 2a). We used five digital cameras to record video through the side windows (Figure S1) at 60 frames per second with a frame size of 1,920 × 1,080 pixels, resulting in a resolution (after correction for minor distortion) of 12 pixels per centimeter (or ~6 pixels per grain). From the videos, water flow depths (H) were calculated by differencing the visually identified top of the static bed, or the top of the sheetflow

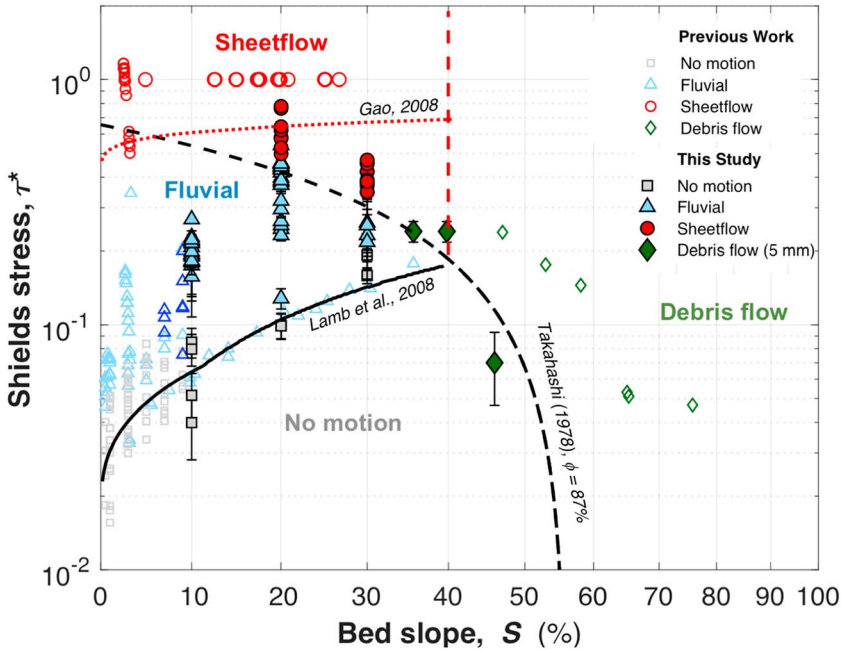

Figure 3. Modes of sediment transport found from our experiments (filled markers ± standard error) and those of Asano (1993), Bathurst et al. (1984), Gao (2008), and Prancevic et al. (2014) (hollow markers).

layer (Figure 2a) if one developed, from the water surface at 20 locations along the test section (Figure S3). Average surface flow velocities (U_{sur}) were calculated from tracking pulses of dye or foam pieces, and from continuity (where $U_{sur} = Q_{sur}/HW$), and these methods agreed within 15%. The nondimensional Shields stress (τ^*) was calculated using

$$\tau^* = \frac{\tau}{(\rho_s - \rho)gD_{50}} \quad (2)$$

where $\tau = \rho g R_h \sin\theta$ and R_h is the hydraulic radius calculated using a sidewall correction depending on the fraction of the banks that were smooth or alluvial (Chiew & Parker, 1994; Vanoni & Brooks, 1957), which changed under different flow conditions with the emergence and evolution of bars. Reported τ^* ranges for each flow condition (no motion, initial motion, etc.) reflect the increments by which the flow was increased. For the experimental runs with planar beds, wall stresses were negligible and $R_h \sim H$.

Particle displacement maps were constructed (Figures 2b and 2c) between successive video frames (every 1/60 s) with a six-pixel correlation window (or approximately one grain diameter) using a dense optical flow algorithm (see the supporting information). From the displacement maps, downstream particle velocities at a given depth z within the bed were calculated by averaging the displacement along a row parallel to the flume bed (extending 15 cm upstream and 15 cm downstream of where we extracted a surface flow depth measurement) and dividing by the elapsed time (1/60 s). Short movie clips (order 1 to 2 s) extracted at the same time as flow depth measurements provided 60 to 120 frames per flow condition and location, resulting in a time-averaged velocity at that location. We then repeated this analysis for 10 locations in the center 3 m of the flume (each sample was taken ~30 cm apart), so that the final average particle velocity at a given depth within the bed, $U_p(z)$, is the result of both time- and space-averaging. The solid fraction of the sheetflow layer or static bed (C_b) was calculated from video images for each flow condition as

$$C_b \sim \frac{1.15 n_p V_p}{A D_{50}} \quad (3)$$

where V_p is the particle volume, which we assume to be spherical; n_p is the number of particles we counted touching the side window within area A (~100 cm^2); and 1.15 accounts for the difference in packing between spheres and natural grains (Bridge, 1981).

To measure S_c, we performed experiments identical to Prancevic et al. (2014) except using gravel from our experiments and a flume width of 18 cm; S_c was found to be ~34%, indicating that initial sediment motion occurred by bed failure, which generated debris flows, for $S \geq 34\%$. To compare our results to the Takahashi (1978) model, 58 dry friction angle measurements were performed using a tilting chute (Prancevic et al., 2014), and these yielded a mean failure-plane friction angle of $\phi_o = 86.9\% \pm 1.01\%$. Porosity of $\eta = 0.40$ was calculated as $1 - \rho_{bulk}/\rho_s$ where ρ_{bulk} is the bulk density of gravel after being hand screeded in the chute. Data were also compiled for comparison from previous flume experiments ($0.1\% \leq S \leq 20\%$; Bathurst et al., 1984; Gao, 2008; Mizuyama, 1981; Prancevic et al., 2014).

3. Results

For 10% bed slope, no motion was observed for $\tau^* \leq 0.09$, initial motion occurred at $\tau^* \sim 0.16$, and for $0.16 < \tau^* < 0.2$ bedload transport occurred, with the development of downstream migrating bars (Figure 3). Upper plane-bed conditions developed for $0.2 < \tau^* < 0.3$, during which the destruction of all

bars was observed and the surface layer of the bed became fully mobile such that nearly all of the surface grains were moving as bedload. Both visually and from our displacement maps, we did not observe sediment motion at depths below one grain diameter deep within the bed for the duration of the experiments. Higher stresses were not investigated due to sediment recirculation limitations. Mass failure of the bed and a transition to debris flow or sheetflow transport at this bed slope was not observed.

For 20% bed slope, no motion was observed for $\tau^* < 0.08$, initial motion occurred at $\tau^* \sim 0.13$, and active bedload transport in the presence of alternate bars occurred at $0.15 < \tau^* < 0.33$. Upper plane-bed conditions developed within the range of $0.5 < \tau^* < 0.78$, except unlike upper plane-bed conditions at $S = 10\%$, sediment transport was visually observed to occur in two modes, namely, dilute bedload transport above a zone of sheetflow (Figure 2a and the supporting information). In the sheetflow layer, moving grains had a concentration ranging from $C_b \sim 0.34$ to 0.45, slightly more dilute than the static bed ($C_b \sim 0.54$ to 0.6). Grain-grain interactions, such as grain collisions and grain-induced shear of underlying grains, in addition to fluid forces, appeared to drive sediment motion. The sheet flow layer thickness (H_g) ranged from 21 to 26 mm (or four to five grain layers), while flow depths of the overriding dilute flow (H) ranged from 23 to 38 mm. Mass failure of the bed was not observed.

At a bed slope of 30%, no motion was observed for $\tau^* < 0.19$, initial motion occurred at $0.21 < \tau^* < 0.28$, and upper plane-bed conditions with sheetflow occurred for $0.35 < \tau^* < 0.47$. The sheetflow layer was thicker at this slope compared to $S = 20\%$, with thicknesses of typically 38 to 51 mm (or 7 to 10 grain diameters) and flow depths (H) were 10 to 14 mm; C_b ranged from 0.34 to 0.45. Again, despite very large τ^*, mass failure of the bed was not observed.

Particle velocities through the granular sheetflow layers decreased linearly with depth in the upper 40% of the sheetflows and followed an approximately logarithmic decay below (Figures 4c and 4d). Maximum particle velocities ($U_{p,\max}$), which occurred at the top of the sheetflow layers (at $z = 0$), ranged from 0.06 to 0.31 m/s (Figure 4c), and were proportional to the shear fluid velocity ($u^* = \sqrt{\frac{\tau}{\rho}}$) such that $U_{p,\max} \sim 1.4u^*$.

Despite differences in bed slope and Shields stress, the sheetflow particle velocity profiles, U_p (z), collapse to a single profile when nondimensionalized (Figure 4d),

$$z^* = 0.39V^* + 0.22 \log V^* + 0.61 \tag{4}$$

where z^* is the nondimensional depth ($z^* = \frac{H_g + z}{H_g}$, where H_g is the sheetflow layer thickness and z is negative with distance into the bed) and V^* is the nondimensional velocity ($V^* = U_p\ (z)/U_{p,\max}$; Figure 4d). Sheetflow thickness, H_g, ranged from 21 to 51 mm; H_g increased with steeper bed slopes and did not correlate independently with Shields number (Figures 4a and 4b).

4. Discussion

The model of Takahashi (1978) predicts that bed failure should occur at $\tau^* = 0.55$ for $S = 10\%$, $\tau^* = 0.43$ for $S = 20\%$, and at $\tau^* = 0.3$ for $S = 30\%$. In our experiments, we were unable to reach $\tau^* = 0.55$ at $S = 10\%$; however, Mizuyama (1981) showed that for $\tau^* \rightarrow 1$ with uniform gravels at similar slopes, bed failure and debris flow generation did not occur (Figure 3). In our experiments, we did exceed the proposed thresholds for bed failure at 20% and 30% bed gradients; however, we also did not observe mass failure of the bed and debris flow formation. Instead, we observed the development of upper plane-bed conditions and granular sheetflow at high Shields numbers (Figure 3). Unlike debris flows, the sheetflows lacked a well-mixed granular front, had only a relatively thin layer of colliding grains with high solids concentrations (C_b), and were driven in part by the overriding water flow with dilute bedload transport.

Sheetflow has been observed previously, but predominantly on low sloping beds, $S \lesssim 5\%$ (Figure 3), under relatively deep (e.g., $H > 50D_{50}$) unidirectional and oscillating flows (Asano, 1993; Gao, 2008; Nnadi & Wilson, 1992; Pugh & Wilson, 1999). The onset of sheetflow on low bed slopes with unidirectional flow typically occurs for Shields numbers between 0.4 and 1 (e.g., Gao, 2008; Nnadi & Wilson, 1992; Pugh & Wilson, 1999). Relatively few studies have reported the occurrence of sheetflows on steeper slopes with gravels. Smart and Jäggi (1983) observed that for a D_{50} of ~10.5 mm, a flume slope of ~20%, and Shields numbers of ~0.69, the entire bed started to creep together due to fluidization, and they hypothesized that this

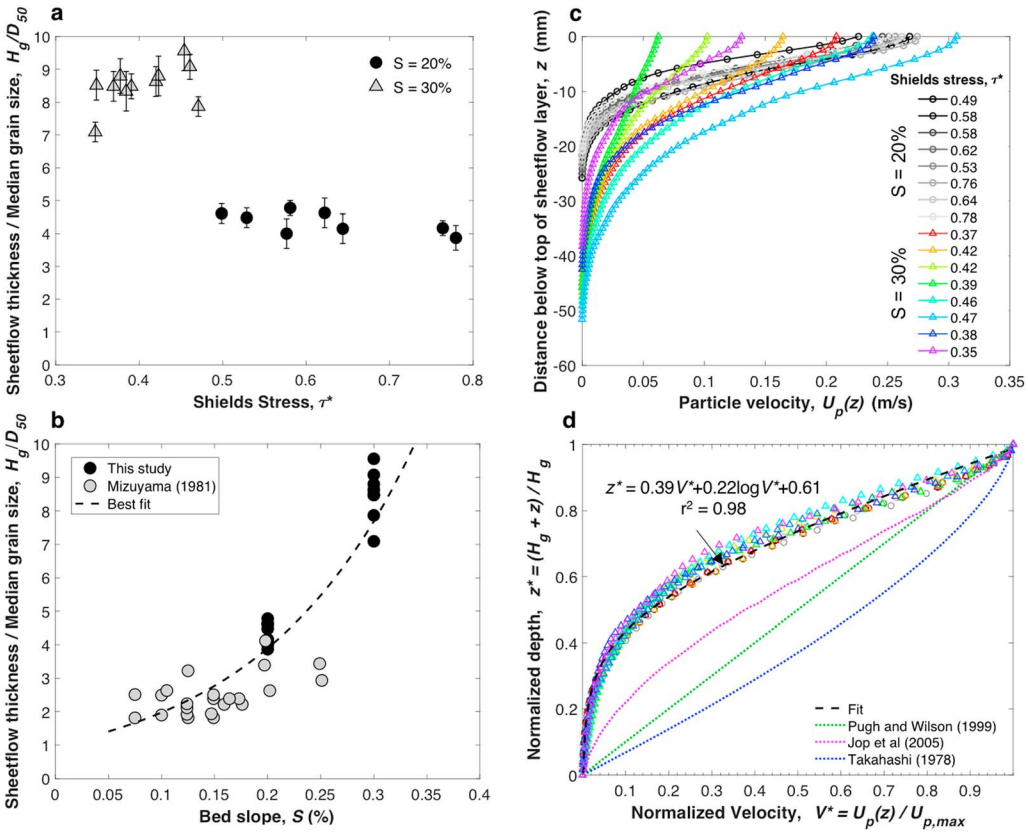

Figure 4. (a) Thickness of sheetflow layer (H_g ± standard error) normalized by median particle size as a function of Shields stress for bed slopes S = 20% (circles) and 30% (triangles). (b) Thickness of sheetflow layer normalized by median particle size as a function of bed slope. (c) Particle velocity profiles within the sheetflow layer for different Shields stresses for bed slopes S = 20% (circles) and 30% (triangles). For each profile, the velocity reported at each depth within the sheetflow layer is the result of the temporally averaged velocity, which is the average of 60 displacement maps generated over 1 s of run time, and the spatially averaged velocity, which is the average of 10 locations in the center of the test section, each separated by ~30 cm. The standard error is less than the size of marker. (d) Nondimensional particle velocity profiles using the same markers as in panel 4c, where the dashed black line is equation (3). Typical profiles for dry granular flows following Jop et al. (2005), sheetflows at low slopes in sand-sized material following Pugh and Wilson (1999), and debris flows following a Bagnold-type profile after Takahashi (1978).

behavior was the transition to a debris flow-like state. They do not report the total bed thickness or whether they had roughness elements on the flume floor to prevent bulk sliding. Mizuyama (1981) also reports a concentrated moving layer that is distinct from fluvial bedload transport. His data show that for $\tau^* > 1$ at $S < 25\%$, granular sheetflow formed in fine gravel.

Our data, as well as data from Mizuyama (1981) and Gao (2008) (Figure 3), suggest that for $S < S_c$ under steady, uniform flow, the transition to sheetflow occurs close to the bed failure prediction of Takahashi (1978) (Figure 3). While Takahashi (1978) does not address sheetflow development, he does suggest that for $26\% < S < 42\%$, bed failure may occur that could be difficult to distinguish from bedload transport. His model assumes that when applied shear stresses (due to parallel seepage and surface flow) overcome resisting stresses within a granular bed at some depth, δ, particles above δ move together, and if $\delta \geq H$, a debris flow occurs due to dispersive pressures from grain-grain contacts that cause mixing throughout the flow depth. At both S = 20% and 30%, we observed sheetflow thicknesses equal to or greater than the overlying fluid depth, but grains did not uniformly mix throughout the depth (see the supporting information), leading to a sheetflow rather than a debris flow. This suggests that dispersive pressures capable of supporting the grains used in these experiments did not develop, possibly due to the granular load being partially supported by frictional rather than collisional particle contacts, dilatancy, or viscous dampening of collisional stresses (Bagnold, 1954; Iverson, 1997; Legros, 2002; Takahashi, 1978), or that another particle support mechanism is required for dispersing grains throughout the dilute overlying flow (e.g., excess pore pressure, increased

buoyancy with the addition of fines, or hindered settling). We also extended the model of Gao (2008), which is primarily a function of excess Shields stress for the onset of sheetflow in sand at low gradient channels, to steeper bed slopes using a slope-dependent critical Shields stress (Lamb et al., 2008), and found that it overestimates the Shields numbers where sheetflows occurred in our experiments (Figure 3). This is likely because this model is based on semiempirical relationships for low-gradient sand transport, where grain-grain contacts are relatively unimportant.

Previous observations and modeling with sand at low bed slopes suggest that the thickness of the sheetflow layer (H_g) is a function of the Shields number and that stresses from the overlying fluid cause deep motion in the bed due to fluid-grain interactions (Lanckriet & Puleo, 2015; Wilson, 1989). In contrast, we found that a steeper bed, rather than greater Shields numbers, led to thicker sheet flows (Figures 4a and 4b). Our finding is similar to dry granular flows down inclined planes, in which the flow thickness is set by the flow rate, and higher flow rates correspond to steeper bed slopes (Jop et al., 2006). This behavior is also similar to a visco-plastic fluid and has been linked to interparticle frictional stresses in granular flows (Forterre & Pouliquen, 2008). Therefore, unlike sheetflows on lower bed slopes where the driving force is dominated by shear from the fluid above, sheetflows on steeper bed slopes might be thicker due to the increased importance of gravity acting on the grains and grain-grain interactions, similar to dry granular avalanches.

Previous work on sheetflows in coarse sand on low gradient beds found that particle velocities within the sheetflow layer (excluding bedload particle velocities) follow roughly linear vertical profiles (Nnadi & Wilson, 1992; Pugh & Wilson, 1999; Wilson, 1989), and maximum particle velocities at the top of the sheetflow layer are ~10u^* (Pugh & Wilson, 1999). In contrast, in debris flow experiments, Kaitna et al. (2014) found that the particle velocity profile was typically concave up for saturated gravel-mud mixtures, similar to that proposed by Takahashi (1978) and Bagnold (1954) (Figure 4d). Dry granular flows follow a similar Bagnold scaling (i.e., $v\,(h) \sim {H_g}^{3/2} - (H_g\text{-}h)^{3/2}$; Figure 4d; e.g., Jop et al., 2005; MiDi, 2004). The particle velocity profiles from sheetflows on steep slopes in our experiments collapse to a self-similar shape that is overall nonlinear, unlike sheetflows on low sloping beds, but not concave up as in debris flows, and more concave down than in dry granular flows. However, the upper ~40% of the sheetflow layer on steep slopes is linear, like sheetflows on low slopes. The profiles in our experiments likely reflect that gravity, fluid shear on the bed, and seepage forces are all important in setting the stress distribution in sheetflows on steep bed slopes.

5. Conclusions

Experiments at bed slopes between $10\% < S < 30\%$ under steady, uniform flows show that sheetflows, rather than debris flows, formed within the high Shields stress range predicted by Takahashi (1978) for bed failure. Our results suggest a change of behavior from sheetflow to channel bed failure as a channel bed steepens under high τ^*, which has implications for predicting sediment fluxes, flow resistance, and channel bed morphology in mountain streams. Sheetflow thickness ranged from 4 to 10 particle diameters, increased on steeper bed slopes, and was not an independent function of the Shields stress, unlike sheetflows at lower bed gradients. Maximum particle velocities within the sheetflows occurred at their upper surface and increased with the fluid bed shear velocity (u^*). Particle velocity profiles within the sheetflow layer were linear in the upper 40% of the flow, like sheetflows on lower slopes, but were concave down below, similar to dry avalanches, which suggests a hybrid behavior where downslope gravitational forces acting on particles, shear from the overriding water, and seepage flow through the granular bed were all important.

Acknowledgments
Funding was provided to M. P. L. by the National Science Foundation grant EAR-1346115 and EAR-1558479 and to M. C. P. by a National Science Foundation Postdoctoral Fellowship EAR-1452337. We thank Samuel Holo, Brian Zdeb, and Erich Herzig for the help with setting up the experiments, collecting data, and calibrating instruments. We thank Francois Ayoub for the help with developing the OpenCV python script used for dense optical flow particle tracking, and Kimberly Hill for insightful discussions. The experimental data are provided in the supporting information.

References

Asano, T. (1993). Observations of granular-fluid mixture under an oscillatory sheet flow. In *Coastal Engineering* (Vol. 1992, pp. 1895–1909). Reston, VA: American Society of Civil Engineers.

Bagnold, R. A. (1954). Experiments on a gravity-free dispersion of large solid spheres in a Newtonian fluid under shear. In *Proceedings of the Royal Society of London A: Mathematical, Physical and Engineering Sciences* (Vol. 225, pp. 49–63). London: The Royal Society. https://doi.org/10.1098/rspa.1954.0186

Bathurst, J., Cao, H., & Graf, W. (1984). Hydraulics and sediment transport in a steep flume: Data from the EPFL study. Report, Centre for Ecology and Hydrology, Wallingford, UK.

Bridge, J. S. (1981). A discussion of Bagnold's (1956) bedload transport theory in relation to recent developments in bedload modelling. *Earth Surface Processes and Landforms*, *6*(2), 187–190. https://doi.org/10.1002/esp.3290060213

Cannon, S. H., Bigio, E. R., & Mine, E. (2001). A process for fire-related debris flow initiation, Cerro Grande fire, New Mexico. *Hydrological Processes*, *15*(15), 3011–3023. https://doi.org/10.1002/hyp.388

Chiew, Y.-M., & Parker, G. (1994). Incipient sediment motion on non-horizontal slopes. *Journal of Hydraulic Research*, *32*(5), 649–660. https://doi.org/10.1080/00221689409498706
Church, M., & Hassan, M. A. (2002). Mobility of bed material in Harris Creek. *Water Resources Research*, *38*(11), 1237. https://doi.org/10.1029/2001WR000753
Forterre, Y., & Pouliquen, O. (2008). Flows of dense granular media. *Annual Review of Fluid Mechanics*, *40*(1), 1–24. https://doi.org/10.1146/annurev.fluid.40.111406.102142
Gao, P. (2008). Transition between two bed-load transport regimes: Saltation and sheet flow. *Journal of Hydraulic Engineering*, *134*(3), 340–349. https://doi.org/10.1061/(ASCE)0733-9429(2008)134:3(340)
Gotoh, H., & Sakai, T. (1997). Numerical simulation of sheetflow as granular material. *Journal of Waterway, Port, Coastal, and Ocean Engineering*, *123*(6), 329–336. https://doi.org/10.1061/(ASCE)0733-950X(1997)123:6(329)
Hanes, D. M., & Bowen, A. J. (1985). A granular-fluid model for steady intense bed-load transport. *Journal of Geophysical Research*, *90*(C5), 9149–9158. https://doi.org/10.1029/JC090iC05p09149
Imaizumi, F., Tsuchiya, S., & Ohsaka, O. (2016). Field observations of debris-flow initiation processes on sediment deposits in a previous deep-seated landslide site. *Journal of Mountain Science*, *13*(2), 213–222.
Iverson, R. M. (1997). The physics of debris flows. *Reviews of Geophysics*, *35*(3), 245–296. https://doi.org/10.1029/97RG00426
Jakob, M., Hungr, O., & Jakob, D. M. (2005). *Debris-flow hazards and related phenomena* (Vol. 739). Berlin, Heidelberg: Springer.
Johnson, C. G., Kokelaar, B. P., Iverson, R. M., Logan, M., LaHusen, R. G., & Gray, J. M. N. T. (2012). Grain-size segregation and levee formation in geophysical mass flows. *Journal of Geophysical Research*, *117*, F01032. https://doi.org/10.1029/2011JF002185
Jop, P., Forterre, Y., & Pouliquen, O. (2005). Crucial role of sidewalls in granular surface flows: Consequences for the rheology. *Journal of Fluid Mechanics*, *541*(1), 167–192. https://doi.org/10.1017/S0022112005005987
Jop, P., Forterre, Y., & Pouliquen, O. (2006). A constitutive law for dense granular flows. ArXiv Preprint Cond-Mat/0612110.
Kaitna, R., Dietrich, W. E., & Hsu, L. (2014). Surface slopes, velocity profiles and fluid pressure in coarse-grained debris flows saturated with water and mud. *Journal of Fluid Mechanics*, *741*, 377–403. https://doi.org/10.1017/jfm.2013.675
Kaitna, R., Palucis, M. C., Yohannes, B., Hill, K. M., & Dietrich, W. E. (2016). Effects of coarse grain size distribution and fine particle content on pore fluid pressure and shear behavior in experimental debris flows. *Journal of Geophysical Research: Earth Surface*, *121*, 415–441. https://doi.org/10.1002/2015JF003725
Lamb, M. P., Brun, F., & Fuller, B. M. (2017a). Direct measurements of lift and drag on shallowly submerged cobbles in steep streams: Implications for flow resistance and sediment transport. *Water Resources Research*, *53*, 7607–7629. https://doi.org/10.1002/2017WR020883
Lamb, M. P., Brun, F., & Fuller, B. M. (2017b). Hydrodynamics of steep streams with planar coarse-grained beds: Turbulence, flow resistance, and implications for sediment transport. *Water Resources Research*, *53*, 2240–2263. https://doi.org/10.1002/2016WR019579
Lamb, M. P., Dietrich, W. E., & Venditti, J. G. (2008). Is the critical Shields stress for incipient sediment motion dependent on channel-bed slope? *Journal of Geophysical Research*, *113*, F02008. https://doi.org/10.1029/2007JF000831
Lamb, M. P., & Fonstad, M. A. (2010). Rapid formation of a modern bedrock canyon by a single flood event. *Nature Geoscience*, *3*(7), 477–481. https://doi.org/10.1038/ngeo894
Lanckriet, T., & Puleo, J. A. (2015). A semianalytical model for sheet flow layer thickness with application to the swash zone. *Journal of Geophysical Research: Oceans*, *120*, 1333–1352. https://doi.org/10.1002/2014JC010378
Legros, F. (2002). Can dispersive pressure cause inverse grading in grain flows? *Journal of Sedimentary Research*, *72*(1), 166–170.
Mao, L., Uyttendaele, G. P., Iroumé, A., & Lenzi, M. A. (2008). Field based analysis of sediment entrainment in two high gradient streams located in Alpine and Andine environments. *Geomorphology*, *93*(3-4), 368–383. https://doi.org/10.1016/j.geomorph.2007.03.008
McArdell, B. W., Bartelt, P., & Kowalski, J. (2007). Field observations of basal forces and fluid pore pressure in a debris flow. *Geophysical Research Letters*, *34*, L07406. https://doi.org/10.1029/2006GL029183
MiDi, G. (2004). On dense granular flows. *European Physical Journal E: Soft Matter*, *14*(4).
Mizuyama, T. (1981). An intermediate phenomenon between debris flow and bed load transport. In *Erosion and Sediment Transport in Pacific Rim Steeplands*, *International Association of Hydrological Sciences* (Vol. 132, pp. 212–224).
Montgomery, D. R., & Brandon, M. T. (2002). Topographic controls on erosion rates in tectonically active mountain ranges. *Earth and Planetary Science Letters*, *201*(3-4), 481–489. https://doi.org/10.1016/S0012-821X(02)00725-2
Montgomery, D. R., & Buffington, J. M. (1997). Channel-reach morphology in mountain drainage basins. *Geological Society of America Bulletin*, *109*(5), 596–611. https://doi.org/10.1130/0016-7606(1997)109%3C0596:CRMIMD%3E2.3.CO;2
Nnadi, F. N., & Wilson, K. C. (1992). Motion of contact-load particles at high shear stress. *Journal of Hydraulic Engineering*, *118*(12), 1670–1684. https://doi.org/10.1061/(ASCE)0733-9429(1992)118:12(1670)
Palucis, M., & Lamb, M. (2017). What controls channel form in steep mountain streams? *Geophysical Research Letters*, *44*, 7245–7255. https://doi.org/10.1002/2017GL074198
Pierson, T. C. (1981). Dominant particle support mechanisms in debris flows at Mt Thomas, New Zealand, and implications for flow mobility. *Sedimentology*, *28*(1), 49–60. https://doi.org/10.1111/j.1365-3091.1981.tb01662.x
Prancevic, J. P., Lamb, M. P., & Fuller, B. M. (2014). Incipient sediment motion across the river to debris-flow transition. *Geology*, *42*(3), 191–194. https://doi.org/10.1130/G34927.1
Pugh, F. J., & Wilson, K. C. (1999). Velocity and concentration distributions in sheet flow above plane beds. *Journal of Hydraulic Engineering*, *125*(2), 117–125. https://doi.org/10.1061/(ASCE)0733-9429(1999)125:2(117)
Recking, A. (2009). Theoretical development on the effects of changing flow hydraulics on incipient bed load motion. *Water Resources Research*, *45*, W04401. https://doi.org/10.1029/2008WR006826
Schneider, J. M., Rickenmann, D., Turowski, J. M., Bunte, K., & Kirchner, J. W. (2015). Applicability of bed load transport models for mixed-size sediments in steep streams considering macro-roughness. *Water Resources Research*, *51*, 5260–5283. https://doi.org/10.1002/2014WR016417
Smart, G. M., & Jäggi, M. (1983). Sedimenttransport in steilen Gerinnen: Sediment transport on steep slopes. Versuchsanst. für Wasserbau, Hydrologie u. Glaziologie an d. Eidgenöss. Techn. Hochsch.
Stock, J., & Dietrich, W. E. (2003). Valley incision by debris flows: Evidence of a topographic signature. *Water Resources Research*, *39*(4), 1089. https://doi.org/10.1029/2001WR001057
Sumer, B. M., Kozakiewicz, A., Fredsøe, J., & Deigaard, R. (1996). Velocity and concentration profiles in sheet-flow layer of movable bed. *Journal of Hydraulic Engineering*, *122*(10), 549–558. https://doi.org/10.1061/(ASCE)0733-9429(1996)122:10(549)
Takahashi, T. (1978). Mechanical characteristics of debris flow. *Journal of the Hydraulics Division*, *104*(8), 1153–1169.
Trampush, S. M., Huzurbazar, S., & McElroy, B. (2014). Empirical assessment of theory for bankfull characteristics of alluvial channels. *Water Resources Research*, *50*, 9211–9220. https://doi.org/10.1002/2014WR015597

Vanoni, V. A., & Brooks, N. H. (1957). Laboratory studies of the roughness and suspended load of alluvial streams. Report to Corps of Engineers, U.S. Army, Missouri River Division, Report No. E-68.

Wilson, K. (1989). Friction of wave-induced sheet flow. *Coastal Engineering*, *12*(4), 371–379. https://doi.org/10.1016/0378-3839(89)90013-6

Yager, E. M., Turowski, J. M., Rickenmann, D., & McArdell, B. W. (2012). Sediment supply, grain protrusion, and bedload transport in mountain streams. *Geophysical Research Letters*, *39*, L10402. https://doi.org/10.1029/2012GL051654